Materials Today Communications 33 (2022) 104583

Contents lists available at ScienceDirect

Materials Today Communications

journal homepage: www.elsevier.com/locate/mtcomm

Corrosion mechanism of Ti-6Al-4V morse taper dental implants connected to 316 L stainless steel prosthetic abutment

Larissa Oliveira Berbel *, Bárbara Victoria Gonçalves de Viveiros, Ana Lígia Piza Micelli, Frederico Nigro, Jesualdo Luiz Rossi, Isolda Costa

Instituto de Pesquisas Energéticas e Nucleares, IPEN-CNEN/SP, Av. Prof. Lineu Prestes, 2242, 05508-000 Sao Paulo, SP, Brazil

ARTICLE INFO

Keywords:
Dental implants
Stainless steel
Ti6Al4V
Morse taper
Corrosion

ABSTRACT

The aim of this work was to investigate the effect of galvanic coupling between stainless steel AISI 316 L abutment type Morse taper and implant made of ASTM F1108–14 Ti-6Al-4V alloy. The assembly of the two alloys was carried out using mechanical imbrication by means of successive strikes at 0.05 J force onto the abutment inserted in the implant along the centerline. Corrosion attack at the interface of the alloys was evaluated according to the number of strikes used for joining the parts. Corrosion resistance was evaluated for the samples by open circuit potential measurements as function of time and scanning vibrating electrode technique (SVET) and scanning ion selective electrode technique (SIET) in phosphate buffer solution with pH adjusted to 3.0, and into which hydrogen peroxide was added to simulate tissue inflammatory conditions. Samples were evaluated at the cross and longitudinal sections. Results indicated that the number of strikes used in assembling affected corrosion susceptibility. The lowest amount of corrosion products was associated to the highest number of strikes used. The corrosion resistance was related to the characteristics of the crevice between the implant and the abutment.

1. Introduction

Dental implants were designed with the aim of improving the masticatory and aesthetic functions of edentulous patients. In order to use metallic materials in the manufacture of dental prostheses, implants had to meet certain properties to be safely inserted into the human body, such as high mechanical strength, biocompatibility and corrosion resistance [1–3].

The materials used in the manufacture of prosthetic pillars can be of different types, such as gold alloy, silver-palladium, nickel-chromium, cobalt-chromium, stainless steel and also titanium and its alloys [4]. However, when two or more of these materials are in electrical contact, they present risks of undergoing galvanic corrosion. This is due to the oral region being able to act as an accelerator of the corrosion process due to the aggressiveness of the medium, including pH changes, variation of oxygen concentration, presence of microorganisms, mechanical stress and, eventually, harsh conditions due to inflammation processes [4–6].

In order for implants to present high durability, one of the most important factors is the way in which the connection between the abutment and the implant is made. This connection must be carried out according to the torque indicated by the manufacturer of the implant, thus providing a correct fitting of the parts thus minimizing the problems in the gap region between them [3].

Implant and prosthetic abutment subjected to stress might be deformed and consequently, loosening of the connection might occur. This effect can lead to infiltration by saliva, microorganisms, glycoproteins and other components of body fluids. This infiltration into the inner part of the implant results in it acting as a reservoir for commensal and/or pathogenic bacteria, mainly anaerobic bacteria, due to low oxygen availability. Consequently, it can result in inflammation of the peri-implant tissue and, consequently, bone resorption [5–11].

A prosthetic abutment connection fastened with a tapered interference fit allows the part to be angled, providing better planning and positioning of the dental implant according to the bone quality of the patient. The angulation of the abutment leads to accentuated plastic deformation, hindering the use of titanium alloys and requiring materials with higher straining capacity so that the metallurgical and mechanical quality of the set is not affected [3]. A material that can be used in the manufacture of such pillars is the AISI 316 L stainless steel.

* Corresponding author.
E-mail addresses: lari_berbel@yahoo.com.br (L.O. Berbel), barbaravictoriaviveiros@gmail.com (B.V.G. Viveiros), analigiamicelli@hotmail.com (A.L.P. Micelli), nigro6@terra.com.br (F. Nigro), jelrossi@ipen.br (J.L. Rossi), icosta@ipen.br (I. Costa).

https://doi.org/10.1016/j.mtcomm.2022.104583
Received 23 March 2022; Received in revised form 4 September 2022; Accepted 29 September 2022
Available online 1 October 2022

Dental implants are placed in the oral region with the platform of the implant at or under the level of the alveolar bone crest, and the region of the pillar-implant interface is exposed to body fluids. Consequently, the implants may suffer bacterial infiltration due to the gap between the abutment and the implant [12]. Different types of implant systems are observed with different connections of the implant-abutment interface. An important factor of implant-abutment connections is its watertightness and consequently biological stability by preventing the entry of saliva and bacteria into the internal region of the implant. This can be achieved by different types of sealing.

The Morse taper connection represents an alternative to the internal and external hexagonal connections [13]. Through the superposition of the components of the implant-abutment system, a better fit between the parts is obtained, providing a smaller gap and, consequently, influencing bacterial infiltration; in addition, it minimizes abutment loosening and improves mechanical stability, decreasing peri-implant bone resorption [14–16]. However, studies in the literature show that bacterial and body fluid infiltration can occur in Morse taper implants [17–20].

In their study, Harder et al. [19] evaluated the sealing capacity of conical connections inoculated with lipopolysaccharides (LPS) in order to assess microleakage in the gap region between implants. LPS was used due to its small molecular size which is capable of penetrating into very small spaces. The results showed that microleakage at the molecular level might occur in the microgap between the implant and the abutment, using the torque recommended by the manufacturer and under static conditions; this effect could be more significant when the implant was subjected to cyclic loading.

Faria et al. [21] compared the contamination of the internal parts of different types of implants (external hexagonal, internal hexagonal and Morse tapered connection) inoculated with *Escherichia coli*. The samples remained in a test tube for a period of 7 days. After this period, the samples that resulted in turbidity in the solution were transferred to a Petri dish containing TSA (tryptic soy agar) and incubated at 37 °C for 24 h to assess bacterial viability. The results obtained showed the presence of a low level of contamination at the abutment-implant interface and the amount of bacterial infiltration was similar in all types of connections studied.

The size of the gap between the prosthetic abutment and the implant tends to increase the probability of bacterial colonization and its accommodation inside the implant, leading to local acidification and inflammatory conditions [22]. One of the most frequent inflammatory processes in patients with dental implants is peri-implantitis, which affects the soft and hard tissue around the implant, causing bone resorption which, in the long term, can lead to implant failure [22].

In addition, the abutment-implant interface region has low access to oxygen, which can trigger crevice corrosion. In this type of corrosion, local acidification occurs, which can accelerate the corrosion process. When an implant-abutment connection is manufactured with different alloys, this assembly is also susceptible to galvanic corrosion due to potential differences between the alloys, creating an in vivo galvanic cell [21,23,24].

Despite the high corrosion resistance required by metallic materials used in the manufacture of dental implants, the aggressiveness of the medium can cause damage to the passive oxide layer that is usually found on the material surface of biometallic materials. The breakdown of the passive layer is followed by degradation of the exposed metal [25,26]. Chloride ions are aggressive species to oxide films favoring its breakdown mainly at the weakest sites of the passive layer. The weakest sites are related to discontinuities in the oxide film due to heterogeneities in the alloy microstructure, mainly due to the presence of precipitates formed during the solidification of the alloy. The cleanest is the microstructure of the alloy the more resistant is the oxide film.

There are many studies on the corrosion of Ti alloy used as dental implants [1,2,4,27,28]. However, few studies investigated stainless steel for this type of application [29,30], and, to our knowledge, there is no previous published work on the effect of galvanic coupling stainless steel and Ti alloy and exposing them to conditions that simulate the oral environment. Once the combination of the two materials is considered for use as dental implants, it is important to evaluate their corrosion behavior when exposed to the aggressiveness of the buccal medium. This investigation intends to contribute with new knowledge on the corrosion behavior of these two alloys when galvanically coupled.

The objective of this work was to study the corrosion mechanism between the assembled alloys, titanium alloy ASTM F1108–14 Gr 5 (Ti-6Al-4V) [31,32] as an implant and stainless steel (SS) AISI 316 L, as a prosthetic abutment connected with 3, 5 and 7 strikes at 0.05 J force, in a solution of phosphate buffered saline (PBS) at acidic pH, in the presence of hydrogen peroxide which acts as a substitute for reactive oxygen species (ROS) typical of inflammatory conditions [27,28].

2. Materials and methods

2.1. Samples

The Fig. 1 shows the design of a device (striker) used in conjunction with the taper-lock abutment system, which is used for prosthetic teeth. In this system, a titanium implant (see Fig. 1A) is placed in the jaw and bone heals around the implant to anchor it. An abutment, which serves as a post for attaching a prosthetic tooth, is placed in the implant through a taper lock mechanism, the tapered interference fit is used for fastening the two parts. The samples used in the present study, which consisted of a Ti-6Al-4V dental implant with a Morse taper 316 L stainless steel abutment.

2.2. Samples preparation

The prosthetic abutment was fixed to the implant using a striker (Fig. 1A) and different numbers of strikes were used for fixation: 3, 5 and 7 strikes at 0.05 J of energy, according to the manufacturer's specifications [3]. After this step, the samples were embedded in a cold curing resin, in the longitudinal and transversal (cross-section) sections (see Fig. 1B). Surface preparation was carried out prior to the electrochemical tests by sequential grinding the samples on SiC sandpaper with particle sizes of #800, #1200, #2000 and #4000. Subsequently, the surface of the samples was polished with a 1 μm diamond paste; the samples were cleaned in a sonifier for 5 min and dried under hot air stream. Finally, the samples were stored in a desiccator until the time of testing.

2.3. Optical profilometry

In order to assess the size and depth of the gap region between the implant and the abutment, measurements were taken using an optical profilometer focusing on the implant/prosthetic abutment junction with 3 strikes, 5 strikes and 7 strikes.

2.4. Electrochemical characterization

Electrochemical tests were carried out using a phosphate buffer solution with pH adjusted to 3 and with the addition of 1% (v/v) of hydrogen peroxide (H_2O_2) as the electrolyte. Hydrogen peroxide was used to simulate the effects of reactive oxygen species (ROS) [28,33]. The choice of this solution is to mimic inflammatory conditions and typical of gaps, because, within the gap regions between the abutment and the implant, the pH tends to be acidified [24,28]. Prior to the electrochemical tests, the area to be tested was delimited around the gap region ($A = 0.04\ cm^2$) using beeswax in order to avoid gaps between the sample and the resin and also to maintain the same size of the exposed area between alloys, so that it does not influence the electrochemical behavior of the coupling.

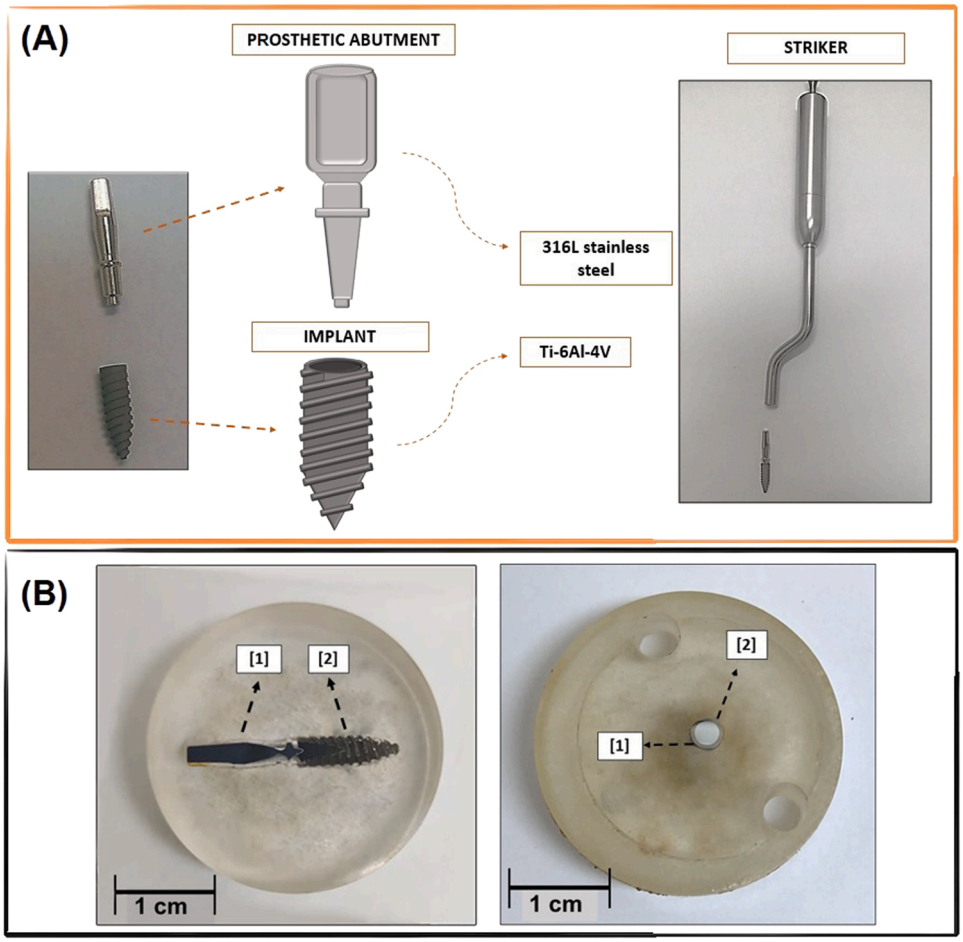

Fig. 1. (A) Samples of Ti-6Al-4V dental implant connected to a 316 L stainless steel prosthetic abutment and the striker used to join the parts and (B) samples after embedding in resin and surface preparation at longitudinal and transversal sections, with a cut off at the implant maximum height region. In (1) the dental implants of Ti-6Al-4V and the abutment in (2).

2.4.1. Open circuit potential measurements

The open circuit potential (OCP) was measured as a function of exposure time using the electrometer of a Gamry Reference 600 + potentiostat until a total time of 24 h. All tests were performed at (25 ± 2) °C, under natural aeration conditions. The electrolyte used was an acidic solution (pH 3.0) of phosphate buffer solution (PBS) whose composition is 8.5 g. L^{-1} NaCl, 1.55 g. L^{-1} Na_2HPO_4 and 0.23 g. L^{-1} NaH_2PO_4 with addition of 1% (v/v) of hydrogen peroxide.

2.4.2. Scanning vibrating electrode technique

Scanning vibrating electrode technique (SVET) was performed by means of *Applicable Electronics™* equipment which was controlled by ASET 4.0 Software (Science Wares™). The vibrating electrode consisted of Pt-Ir electrodes with deposited platinum at the tip. The vibrating electrode was placed at 100 ± 3 μm above the tested surface. Vibration occurred in the perpendicular (Z) and parallel (X) planes with an amplitude of 19 μm. The electrode vibration frequencies were 174 Hz (X) and 73 Hz (Z). The time interval between acquisitions of each current density point was 0.5 s. All experiments were performed at (20 ± 2) °C in a Faraday cage. Maps were obtained every 2 h for a period of 24 h. The electrolyte used in the SVET tests was the same used for OCP measurements, that is, PBS with the addition of 1% (v/v) of hydrogen peroxide and pH adjusted to 3.0.

2.5. Scanning ion-selective electrode technique

Scanning ion-selective electrode technique (SIET) tests were performed using the same equipment used in the SVET tests. The electrode used in this technique is a capillary with an external diameter of 1.5 mm. A micropipette puller equipment (was used to mold the capillary tip into a conical shape. The diameter of this tip was 2 μm. The capillaries were silanized by injecting 200 μL of N, N-dimethyltrimethylsilamine into a preparation chamber at 220 °C. The membrane for selective H^+ microelectrodes was composed of 25 μL of hydrogen ionophore II - cocktail B, and the internal reference solution was composed of a buffer composed of 0.01 mol.L^{-1} of KH_2PO_4 in 0.1 mol. L^{-1} of KCl. A chlorinated silver wire was inserted into the capillary resulting in the selective H^+ microelectrode. An Ag/AgCl electrode with KCl solution was used as an external reference electrode. The H^+ selective microelectrode was calibrated using buffer solutions according to the Nernst equation. The microelectrodes showed stable and reproducible potential in the pH range between 6.9 and 10.6. The Nernst slope was (58.0 ± 0.1) mV/pH.

The selective microelectrode was located (50 ± 3) μm above the surface. All tests were performed in a Faraday cage at (20 ± 2) °C. The electrolyte used in the SIET tests was a PBS solution of pH 7.0 to which 1% (v/v) of hydrogen peroxide was added. The aim of using this solution was to evaluate the effect of corrosion under crevice conditions on the pH of the solution. The test lasted 24 h, and maps were obtained every 2 h.

2.6. Immersion

After surface preparation, the samples for exposure in the

longitudinal section and connected with 3 strikes, 5 strikes and 7 strikes were immersed in PBS adjusted to pH 3.0 with the addition of 1% (v/v) H_2O_2. The exposed surface was observed after periods of 1 day, 4 days and 7 days, and the development of corrosion products was evaluated by surface observation using scanning electron microscopy (SEM). Samples that had their cross-section exposed to the electrolyte were evaluated after 7 days of immersion.

2.7. Scanning electron microscopy and energy dispersive spectroscopy (SEM-EDS)

The surface of the tested samples was observed using scanning electron microscopy (SEM) and the composition of the corrosion products were semi-quantitatively evaluated using energy dispersive spectroscopy, at an accelerating voltage of 15 keV.

3. Results

3.1. Optical profilometry

Fig. 2 shows the results of optical profilometry focusing on the implant/prosthetic abutment junction with 3, 5 and 7 strikes.

The depth of the interface between the alloys (see Fig. 2) showed that there are significant differences in the width and depth of gaps between samples connected with different numbers of strikes. The sample connected with 3 strikes presented a larger gap region, with a width of 80 μm and a depth of 4.50 ± 0.16 μm. The sample with 5 strikes was 70 μm wide and 3.50 ± 0.02 μm deep, while the sample with 7 strikes had a smaller gap between the alloys, with a width of 60 μm and a depth of 3.00 ± 0.07 μm.

3.2. Electrochemical characterization

Fig. 3 shows the variation of open circuit potential with the immersion time for the samples connected with 3 strikes, 5 strikes and 7 strikes and also for 316 L stainless steel and Ti-6Al-4V separately in the acidified electrolyte (pH 3.0).

The OCP results (see Fig. 3) show that among the alloys tested individually, 316 L stainless steel presents higher potentials than the Ti-6Al-4V alloy during almost the entire elapsed time of the test. This shows

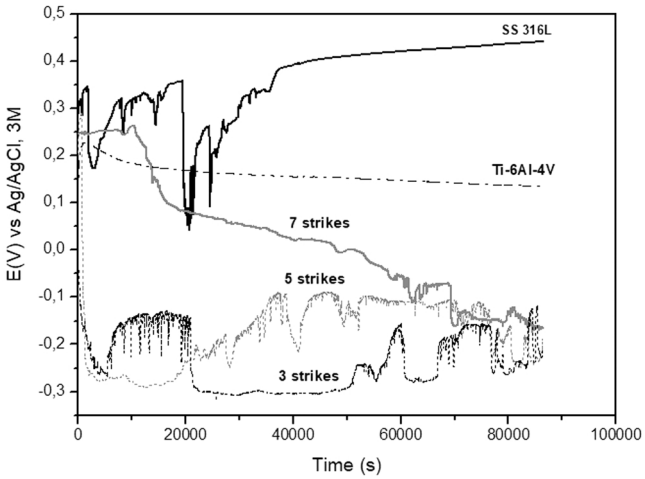

Fig. 3. Open circuit potential variation with immersion time curves for alloys 316 L and Ti-6Al-4V individually tested connected immersed for 24 h in PBS solution with pH adjusted to 3.0.

that the 316 L stainless steel acts as a cathodic region when in contact with the titanium alloy, which will act as an anodic region. It was also observed that the stainless steel alloy presents some potential oscillations in the first 11 h of testing, indicating that this alloy is susceptible to localized corrosion until stabilization. It is important to observe that the direct coupling of 316 L SS and Ti-6Al-4V does not lead to a mixed potential between the materials, but it becomes much more negative than both materials. This means that both materials lose their passive state at least partially, resulting in less compact and even poorly protective hydroxide-containing layers, instead of the protective oxide layers.

Table 1 shows the initial and final values of potential for all tested conditions and it is possible to observe that the potential increases with the number of strikes, that is, for those samples that present a smaller gap region between the parts.

The results in Table 1 clearly demonstrate the effect of the number of strikes for connecting the prosthetic abutment to the dental implant on the electrochemical behavior of the materials. The samples with abutment-implant coupling connected with 3 strikes and 5 strikes

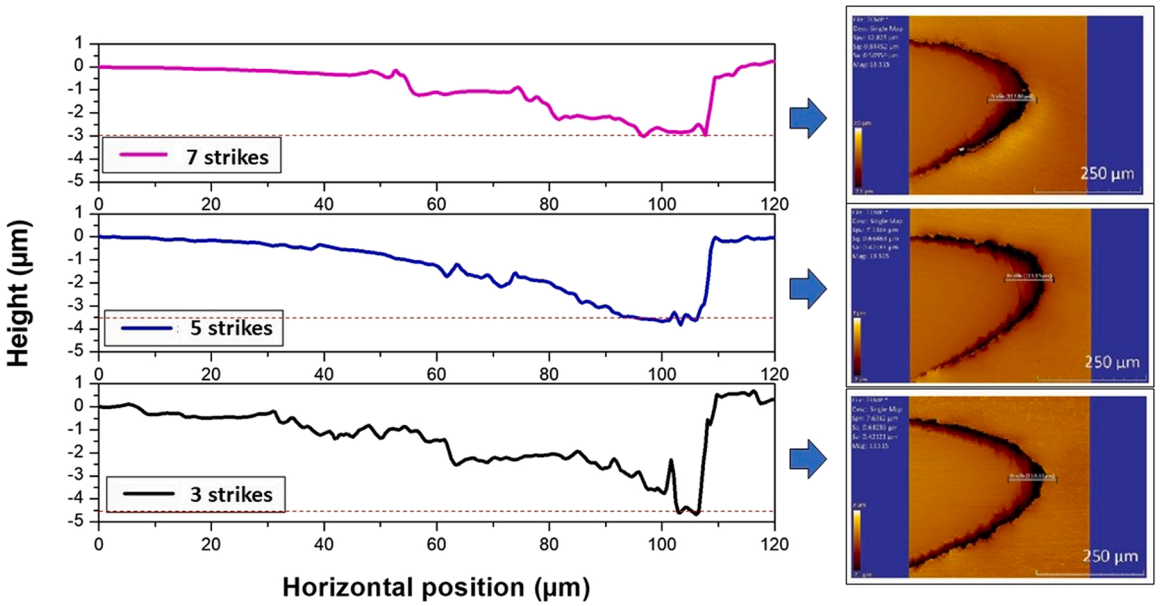

Fig. 2. Optical profilometry of the 316 L stainless steel prosthetic abutment connected to the Ti-6Al-4V dental implant after mechanical joining with 3, 5 and 7 strikes.

Table 1
OCP potentials in mV (initial and after 24 h of exposure (final) exposure to PBS solution at pH 3.0) for the 316 L stainless steel, for the Ti-6Al-4V alloy and for the connected samples by strikes.

	$E_{initial}$ (mV)	E_{final} (mV) 24 h
316 L	308	441
Ti-6Al-4 V	161	136
7 strikes	246	-161
5 strikes	208	-190
3 strikes	-42	-217

presented potential instabilities during the whole test, being this behavior typical of passive film attack and pitting nucleation. The results show that the implant connected with 7 strikes presents nobler potentials with a significant drop after 11.000 s. Among the samples, that connected with 3 strikes presented the greatest potential drop, which occurred in the first minutes of the test, indicating an intense attack on the passive film, mainly at the interface between the abutment and implant. The low potential values of the coupled alloys compared to the two alloys tested separately shows a strong effect of the galvanic coupling on the sample electrochemical behavior. In brief, the high passivity resistance of these materials is compromised by galvanic coupling.

Fig. 4 shows the SVET results for 2 h and 24 h of exposure of the samples corresponding to 3 strikes, 5 strikes and 7 strikes to the acidified electrolyte and the images of surfaces by SEM after SVET tests.

The SVET maps in Fig. 4A show that the lowest electrochemical activity in the first hours of the test is related to 7 strikes sample. For this sample, it is observed that the Ti-6Al-4V alloy acts as preferentially as an anodic area (areas in red) in comparison to 316 L stainless steel. The anodic areas are located mainly in the titanium alloy and not exactly at the interface between the two alloys. There is also anodic activity at the interface region between the alloys (yellow areas). The sample prepared with 5 strikes showed higher proportions of anodic areas (red areas) in the interface region and over the titanium alloy, while the sample with 3 strikes exhibited anodic areas mainly at the interface region.

Fig. 4B shows SVET maps obtained for 24 h of immersion. Note that after 24 h, the electrochemical activity decreased in the samples connected with 3 and 5 strikes, while it increased in the sample with 7 strikes. This fact can be explained by the precipitation of corrosion products originating in the most electrochemically active areas that corresponded to the samples with 3 and 5 strikes, and, consequently, by the formation of a partial barrier between the metallic substrate and the corrosive medium.

Fig. 4 C shows the presence of attacked areas at the interface but also on the surface of the 316 L steel, as indicated by the black arrows. These attacks occur due to local acidification resulting from corrosion reactions located mainly in the gap regions between the two alloys. This region gives rise to conditions typical of crevice with a decrease in local pH and destabilization of the protective oxide on the surface, particularly in the region close to the interface. It is observed that after 24 h of exposure to the corrosive medium of the SVET test, the samples with 7 strikes presented smaller amounts of corrosion products, which is related to the smaller gap between the alloys. As soon as the material (abutment-implant) comes into contact with body fluids, corrosion will start, and the corrosion products tend to deposit in the crevice regions.

Fig. 5 shows the SVET maps of the samples exposing the transverse section connected with 3, 5 and 7 strikes comparing their electrochemical behavior after 2 h, 14 h and 24 h exposure to the acidified electrolyte.

The SVET maps (Fig. 5A) of the transversal section show that since the first hours of testing, the sample connected with 7 strikes showed less electrochemical activity, with a homogeneous distribution of cathodic area (areas in blue) on the stainless steel and decreased the number of red spots with the time of the test. The sample connected with 5 strikes showed anodic areas (red dots) since the first hours of the test, related to a the Ti-6Al-4V alloy but there is no significant increase in the anodic areas, showing a fair stabilization of the corrosion process until 24 h of immersion. On the other hand, the sample prepared with 3 strikes showed increasing evolution of the areas affected by corrosion along the test period with localized attack being seen on the stainless steel after 14 h of test. This is due to the aggressive conditions generated by the corrosion at the interface between the two alloys.

Fig. 5B shows SEM images of the exposed surface of the pillar-implant connection, in the transverse section at maximum implant height, with the abutment inserted with 3 strikes, 5 strikes and 7 strikes. After 24 h of exposure to the electrolyte for SVET test, the exposed surface showed small pits on the surface of stainless steel for samples obtained with 3 strikes and 5 strikes, corroborating the SVET maps.

Fig. 6 shows SEM images the surfaces exposed for 7 days to the acidified electrolyte. The SEM images observed after 24 h of immersion in the electrolyte, leading to a large number of pits at the surface attack of the 316 L stainless steel but also on the titanium alloy for the sample obtained with 3 strikes. There is also evidence of attack on the sample obtained with 5 strikes, but only two spots were seen on the titanium alloy of the sample obtained with 7 strikes. The results show the importance of the size of the gap that leads to crevice, on the corrosion resistance of the galvanically coupled samples. It was clear that the resistance of the samples to localized attack increased with the decreased gap between the two alloys.

3.3. *Surface characterization of immersion tests*

The region affected by corrosion, according to the number of strikes used, can be observed in the SEM images obtained after 1 day, 4 days and 7 days of immersion in the acidified electrolyte, see Fig. 7. This Figure shows the influence of the size of the gap between the two alloys and the corrosion. The sample prepared with 7 strikes presented lower amounts of corrosion products at the interface of the alloys. On the other hand, the sample with 3 strikes showed the greatest volumes of corrosion products deposited among the tested and the products located preferentially on the titanium alloy.

As far as it is known by the authors, there are no reports in the literature of studies on the galvanic corrosion between Ti-6Al-4V alloys and 316 L stainless steel used as dental implants. However, the results of this study suggest that the corrosion mechanism of the samples evaluated in this study, promoting galvanic coupling between a titanium alloy dental implant and a 316 L stainless steel prosthetic abutment, is dependent on the gap/crevice conditions between the two alloys, with crevice corrosion being a significant factor affecting the corrosion behavior at the connection of the alloys. For arrangements that favor crevice conditions at the gap, corrosion initiation and propagation will be stimulated with the consequent accumulation of corrosion products in the interface region between the two alloys. It must be mentioned that the galvanic effects also are mainly effective at the interface between the two alloys.

EDS results evaluated the semi-quantitative composition of the corrosion products after immersion tests, and the spectrum is shown in Fig. 8. EDS allows detection of the largest (above 10% by mass) and smallest elements (around 1–10% by mass) present at the abutment-implant interface, with a detection limit of 0.1% mass [34]. The composition of the spectra was determined and the values are shown in Table 2.

The spectrum in Fig. 8 and Table 2 show that Fe and Ti are the elements present in higher amounts. These are the most abundant elements in the alloys used in this study. Ni, Cr, C and Mo are also elements present in the composition of 316 L stainless steel. The presence of these elements deposited at the pillar-implant interface shows that the two alloys suffered corrosion in contact with the electrolyte, indicating that the predominant corrosion mechanism at the connection of these alloys is crevice corrosion considering that for the sample obtained with 7

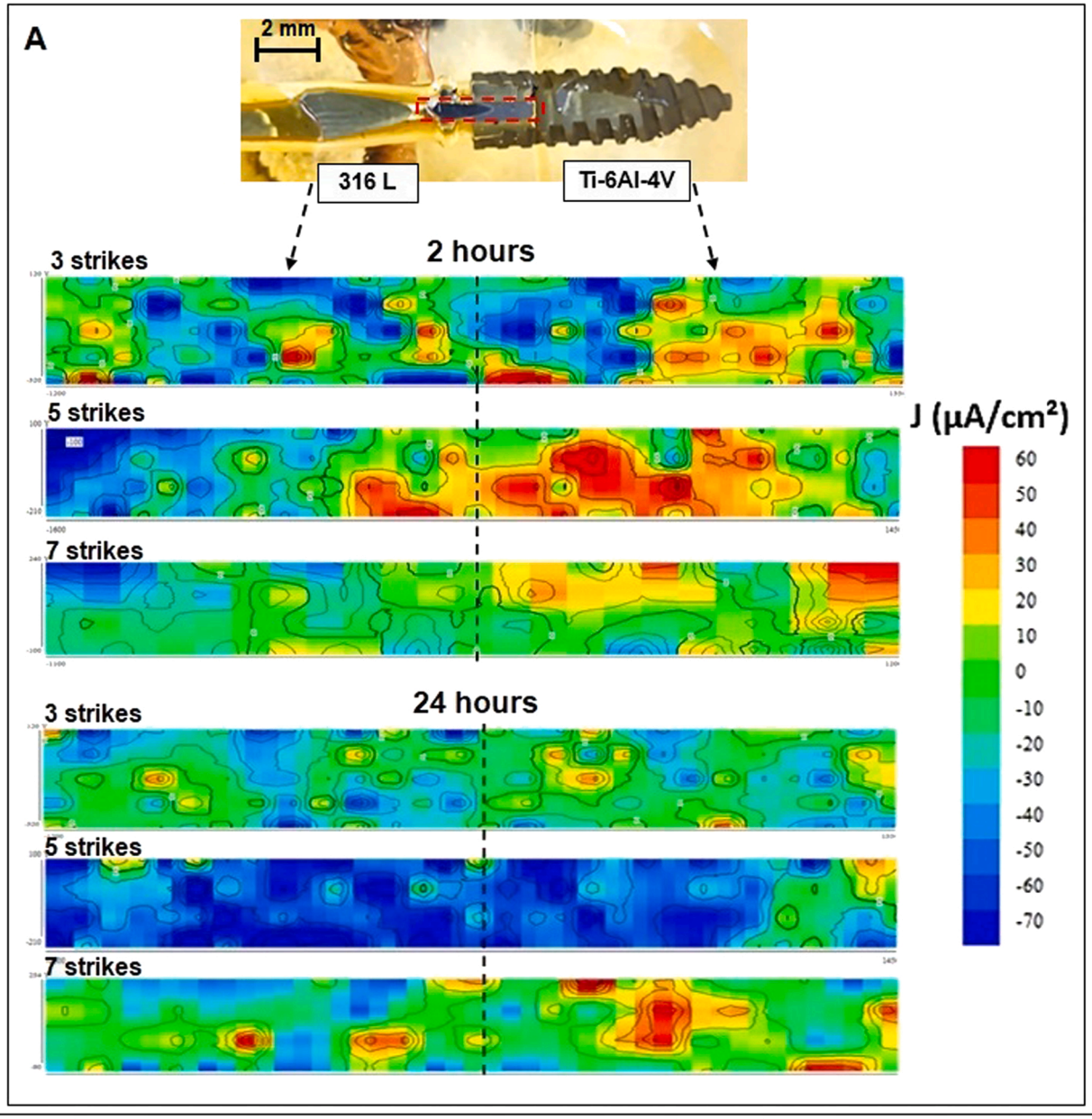

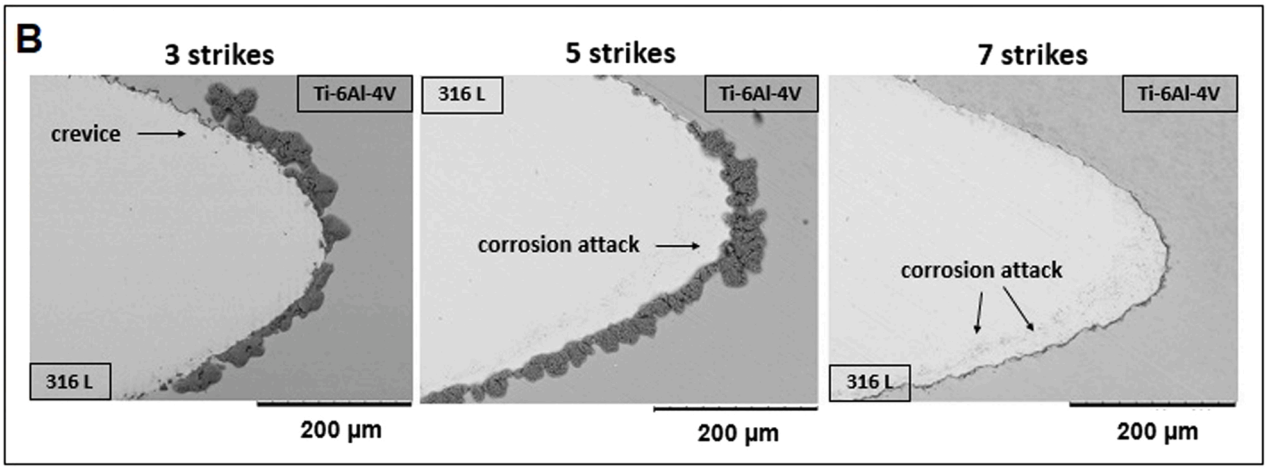

Fig. 4. (A) SVET maps for Ti-6Al-4V alloy (implant) connected to 316 L stainless steel (abutment) corresponding to 3, 5 and 7 strikes, after 2 h and 24 h immersion in PBS (pH 3.0) with 1% (v/v) of H_2O_2. (B) Backscattered electrons scanning images of the interface region between Ti-6Al-4V alloy and 316 L steel for samples obtained with 3, 5 and 7 strikes, after 24 h exposure in PBS solution, (pH 3.0) and with 1% (v/v) of H_2O_2. Area (1×4) mm^2.

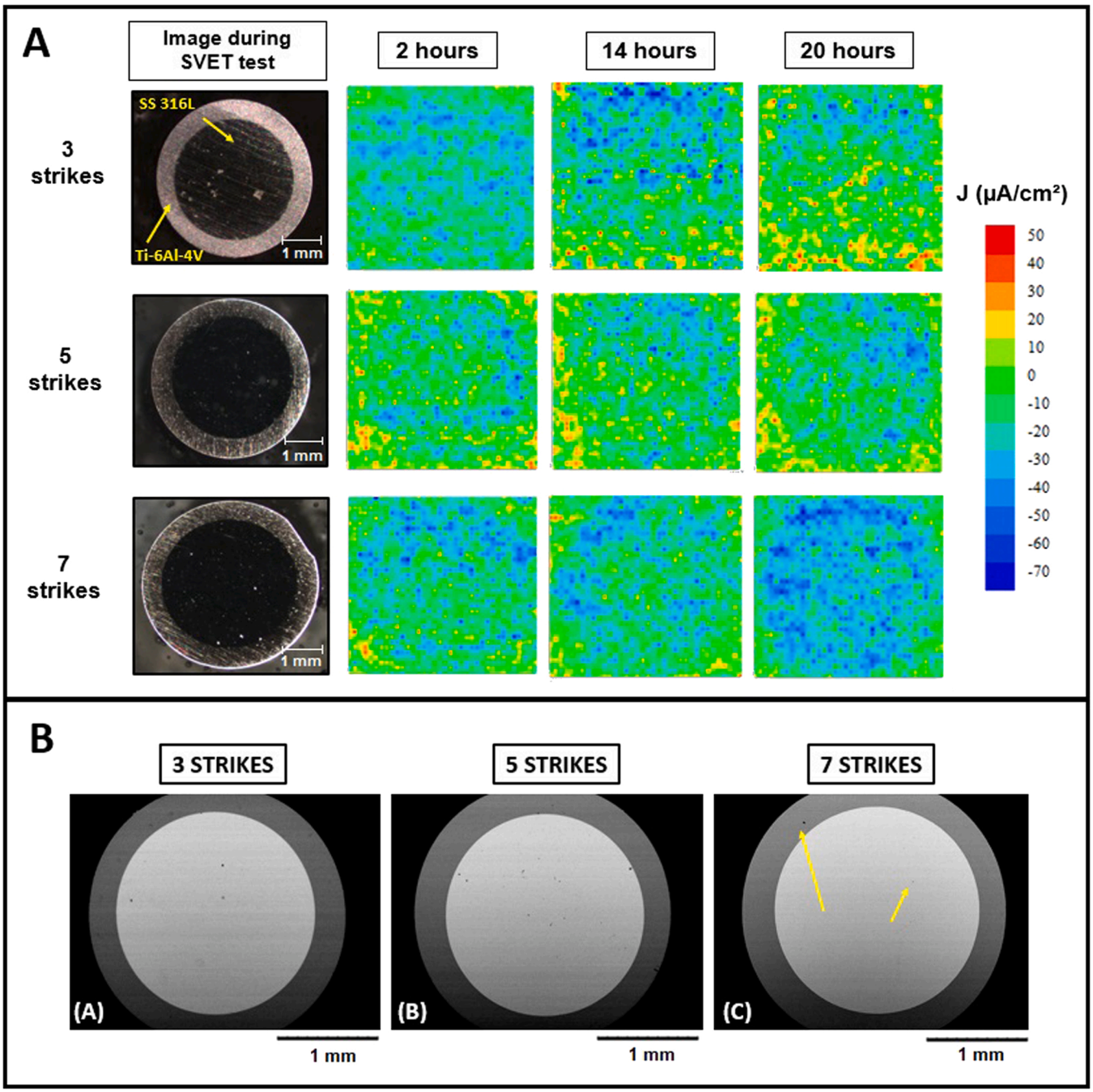

Fig. 5. (A) SVET maps of samples exposing the transversal section of the Ti-6Al-4V alloy (implant) connected to 316 L stainless steel (prosthetic pillar) connected using 3 strikes, 5 strikes and 7 strikes after 2 h, 14 h and 24 h. (B) Backscattered electrons scanning images of the samples obtained with 3 strikes, 5 strikes and 7 strikes with transversal section (cross-section) after 24 h of exposure to the electrolyte. Electrolyte: PBS solution (pH 3.0) and 1% (v /v) of H_2O_2. Area (4×4) mm^2.

strikes, the amount of corrosion products formed was very low.

Vanadium is present in the Ti-6Al-4V alloy and the fact that it was detected in the corrosion product, however, is important to be noted. Vanadium in its elemental condition and as oxides, is toxic to humans, and is associated with osteolysis, neurotoxic effects, neuropathy and osteomalacia [12,35]. Consequently, it is important that the amount of liberated vanadium in the body fluids be very low. Sodium, chlorine and phosphorus are elements present in the phosphate buffer solution (PBS) and, consequently, react with cations originating from corrosion being deposited on the attacked regions.

3.4. Local pH of the gap region

Fig. 9 shows the local pH maps of the samples with a longitudinal section exposed to the neutral electrolyte (pH 7.0) and connected with 3 strikes, 5 strikes and 7 strikes. Due to the highly acidic condition of the solution of pH 3.0, the variations caused by corrosion had no visible effects on pH throughout the test. Therefore, it was necessary to carry out the tests at pH 7.0 to evaluate the effect of the gap that led to crevice conditions on the localized pH of the electrolyte with 1% (v/v) H_2O_2.

The SIET results for the sample connected with 3 strikes (Fig. 9A) show that even after the first minutes of testing, the pH of the electrolyte already presented a rapid decrease, from 7.0 to 5.3, due to the effect of corrosion in the gap/crevice region between the two alloys. This

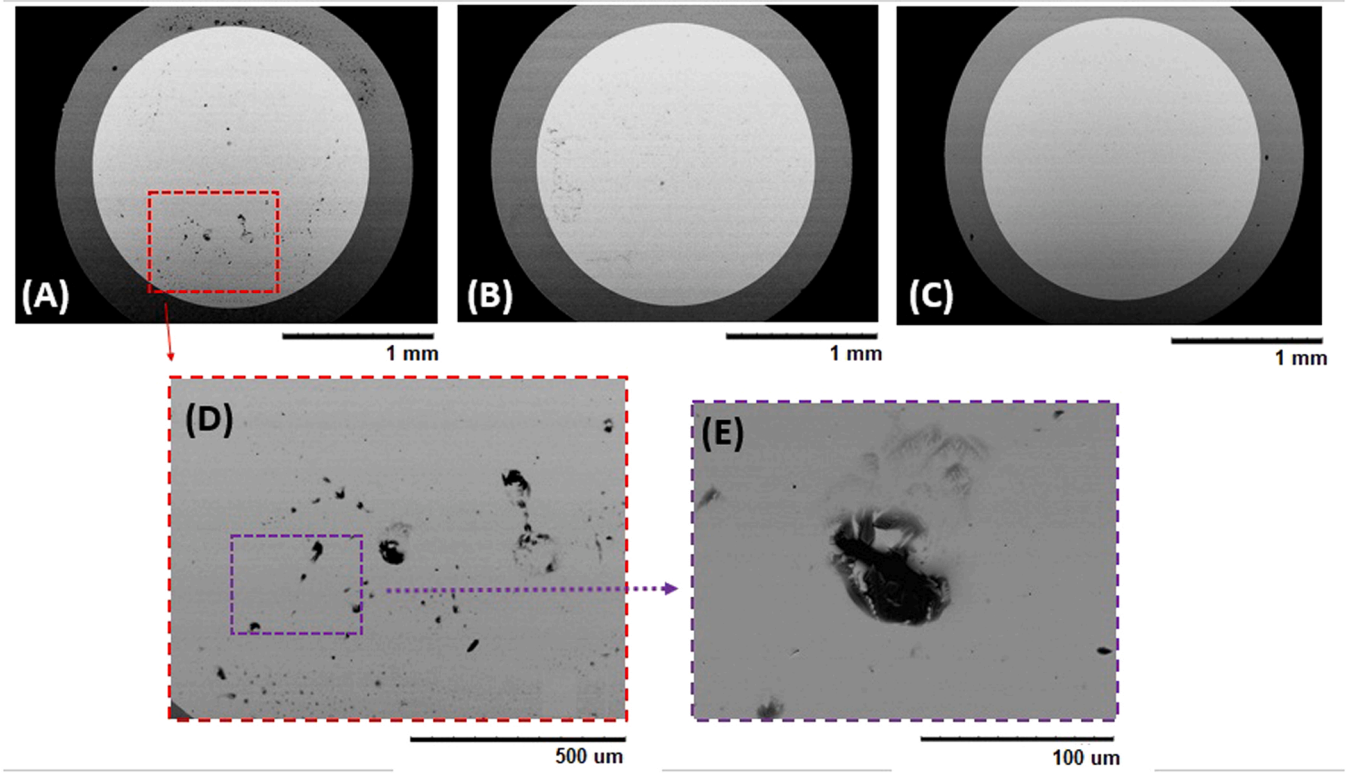

Fig. 6. Backscattered electrons images of samples with transversal section (cross section) exposed to the electrolyte and obtained with (A) 3, (B) 5 and (C) 7 strikes after 7 days of immersion in PBS solution with pH adjusted to 3 and addition of 1% (v/v) H_2O_2. In (D) localized corrosion the 316 L alloy of the sample obtained with 3 strikes and in (E) magnification of (D).

decrease is more significant after 10 h of immersion, with the pH of the electrolyte reaching values of 4.6. For longer periods, there was no further change in the electrolyte in contact with all samples.

The sample connected with 5 strikes (Fig. 9B) shows a pH drop from 6.9 after immersion to 5.3 after 10 h of immersion, showing the effects of localized corrosion on the electrolyte.

Finally, the SIET maps for the sample connected with 7 strikes (Fig. 9C) show that the pH value did not change significantly from the start of exposure (pH 6.8) until 10 h of immersion (6.5), supporting all the previous results presented.

It is important to note that the size of the gap between the abutment and the implant causes changes in surface pH due to the corrosion processes that are taking place within the gap.

4. Discussions

The gap region between the abutment and the implant is more susceptible to corrosion. This occurs due to local acidification between the parts, mainly inserted in the oral region, in which there is a decrease in oxygen flow, making it difficult to restore the passive layer of the metal [24]. Galvanic corrosion occurs when the dental implant and the prosthetic abutment are made of different metals, this type of corrosion occurs when there is saliva infiltration between the implant and the prosthetic abutment, forming a galvanic cell in vivo, due to the potential difference between the metals. This galvanic cell is capable of generating a flow of electrical current through the junction between metals and tissues, causing pain to the patient and also possibly leading to bone destruction [36–38].

In galvanic corrosion, the less noble metal acts as anode (Eq. 1), causing the metal to dissolve when in contact with the corrosive environment, while the metal that has more positive potential (nobler) acts as cathode (Eqs. 2 and 3). All the reactions result in pH changes in the environment close to the samples. In the case of the cathodic regions, the generation of hydroxyl ions or the consumption of hydrogen ions will lead to pH increase, whereas in the anodic regions, the generation of metallic cations will promote water hydrolysis and pH decrease, with acidification of the electrolyte close to the samples [39,40]. If chloride ions are present in the environment, the formation of an acidic medium, according to Eq. 4, will occur.

$$Me \rightarrow M^{n+} + ne^{-} \text{ Anodic} \quad (1)$$

$$O_2 + 4e^{-} + 2\,H_2O \rightarrow 4OH^{-} \text{ Cathodic} \quad (2)$$

$$O_2 + 4\,H^{+} + 4e^{-} \rightarrow 2\,H_2O \text{ Cathodic} \quad (3)$$

$$MCl_n + nH_2O \rightarrow M(OH)_n + nHCl \quad (4)$$

In addition to galvanic corrosion, dental implants can suffer crevice corrosion due to the geometry of the pillar-implant interface, where local oxygen depletion occurs and the concentration of metallic ions increases in the solution with contact with the anodic areas. The exposed metallic material in contact with a solution of different oxygen concentrations will lead to differential aeration cells which are favored when the solution contains chloride ions [36–38].

Crevice corrosion occurs when the oxygen in the region of solution where oxygen replacement is difficult has its oxygen consumed. As the region is occluded, oxygen renewal is difficult leading to metal oxidation and predominance of positive charges in solution (H^{+}). As the oxygen is consumed, the anodic reaction is maintained, generating a high concentration of positively charged ions (M^{n+}), the metal cations favors water hydrolysis and once the metal cations react with hydroxyl ions, there is imbalance of H^{+} in solution. Due to a balance of positive charges in that part of the solution, chloride ions (Cl^{-}) will migrate to the gap region, with the consequent formation of MCl_n. Chloride ions will undergo hydrolysis by water, forming a metal hydroxide and an acid (HCl), as observed in Eq. 4 [35–38,40–42]. Hydrolysis results in acidification within the gap as seen in the SIET results of this study, hence the

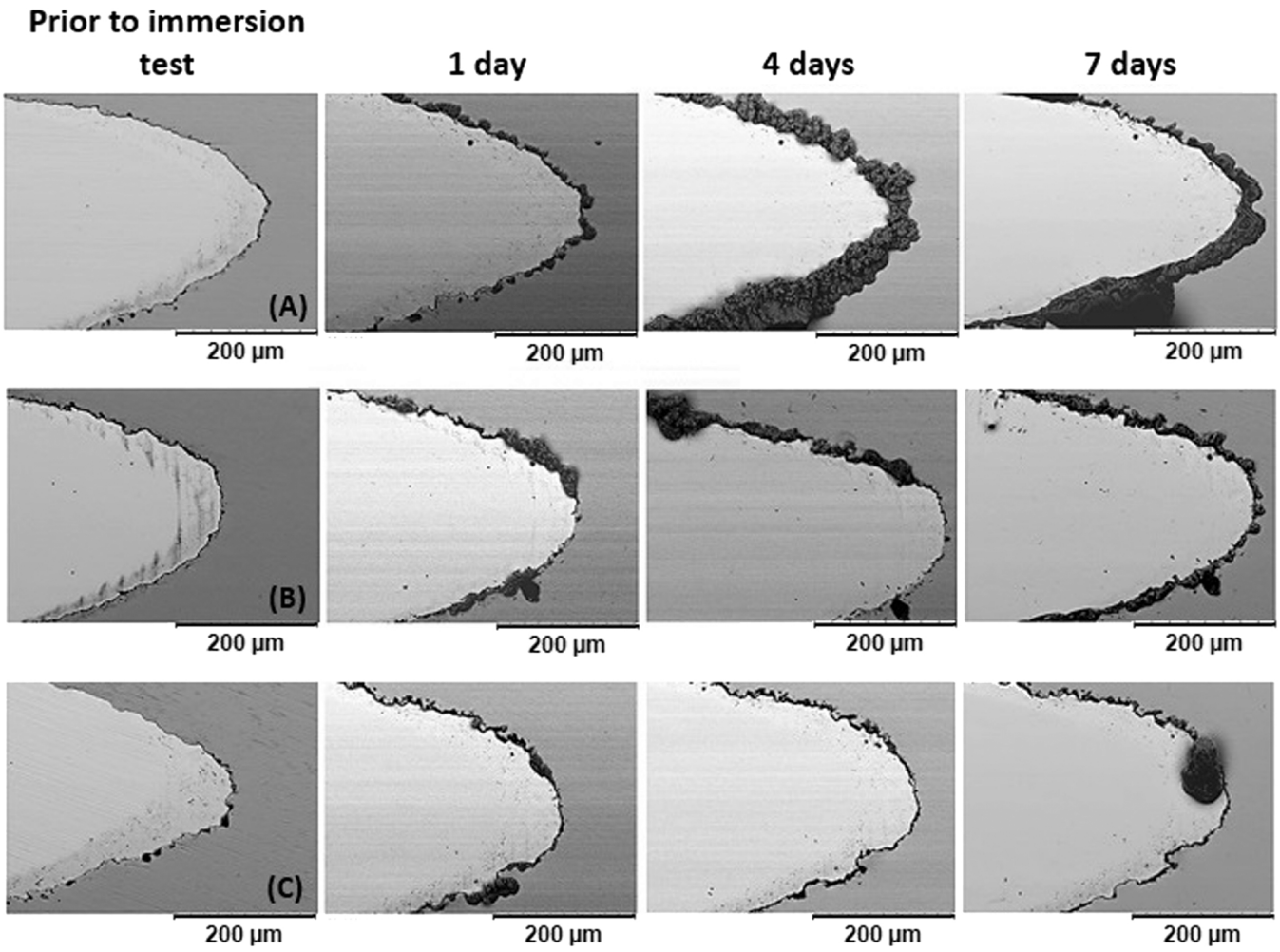

Fig. 7. Backscattered electrons scanning images of the connection between titanium alloys and 316 L stainless steel, in the longitudinal direction, with (A) 3, (B) 5 and (C) 7 strikes, after immersion for 1 day, 4 days and 7 days in PBS solution, with adjusted pH in 3.0 and addition of 1% (v/v) of H_2O_2.

deposition of corrosion products, as seen in the SEM images.

The role of Cl ions in the crevice corrosion related to the joint of implant-abutment is similar to that of these ions on pitting corrosion. Chloride ions are adsorbed on the oxide film decreasing its protective nature and favoring film breakdown. Once the crevice is a region of low access to oxygen, if the passivating oxide film is broken at its weakest sites, its restoration is hindered by the difficult access of oxygen to the interior of the crevice. Thus, a differential aeration cell is formed between the exposed areas and the inner parts of the crevice promoting corrosion propagation. Ti alloys are more resistant against chloride ion attacks than stainless steel because Titanium oxides present improved protective properties compared to the passive oxide on stainless steel resulting in a surface film that is highly resistant to chloride attack. The higher corrosion resistance of Ti alloys in chloride-containing environments compared to stainless steel is due to the Ti alloys microstructures that present a lower amount of heterogeneities at the surface, such as precipitates and second phases, than the stainless steel.

Fig. 10 illustrates the crevice corrosion mechanism starting at the gap/crevice region presenting lower oxygen concentration than the areas with free access to oxygen, and thus, resulting in potential differences between the two areas which lead to corrosion initiation, that is, dissolution of metal at the anodic sites (Eq. 3).

Al'Otaibi et al. [43] evaluated the corrosion behavior of dental implants in the presence of artificial saliva using two dissimilar titanium implants Ti $_{cp}$ and Ti-6Al-4V coupled to a Co-Cr prosthetic abutment and electrochemical tests revealed that, with increasing immersion time, corrosion attack by artificial saliva increased with time on the surface of the coupled metals. In the present study, increased amounts of corrosion products were observed for the samples with gaps that acted as crevices between the titanium alloy and 316 L stainless steel with the increased test time, corroborating the results of Al'Otaibi et al. [43].

Reclaru et al. [44] performed in vitro study of 15 prosthetic alloys, including gold-based alloys, palladium-based alloys and non-precious alloys coupled to Ti_{cp}, forming galvanic coupling. The potential values of the alloys separately, and of the coupling with titanium, were evaluated by open circuit potential measurements and showed that the precious alloys presented higher potentials than titanium or titanium alloy resulting in corrosion attack of titanium. Non-precious alloys, on the other hand, presented lower potentials than the Ti_{cp} or Ti alloy, thus, the last materials will act as cathodes.

Mellado-Valero et al. [45] evaluated the galvanic corrosion behavior of five dental implants made with different materials, specifically, Co-Cr, Ni-Cr-Ti, gold and Ti-6Al-4V alloys, all coupled to a Ti grade 2 alloy, in various solutions, specifically, artificial saliva, and acidic solutions, either with or without fluoride ions. The open circuit potential measurements showed that Au in contact with Ti_{cp} presented a nobler potential while the Co-Cr alloy exhibited more negative potential in artificial saliva solution without fluoride. The results obtained in artificial saliva containing fluoride ions showed that Au also presents a nobler potential in this medium, with the most negative potentials being observed for the titanium alloy. The study showed that galvanic corrosion is dependent on the conditions of the environment and the materials

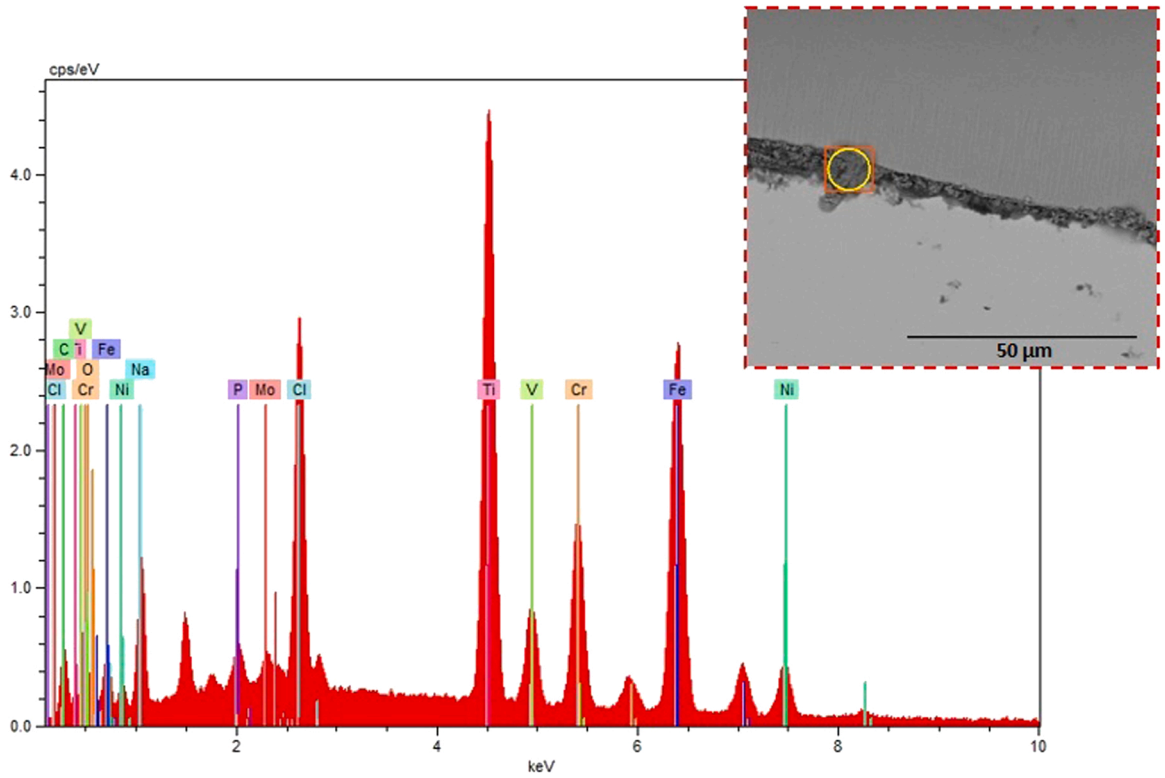

Fig. 8. EDS spectrum obtained in a scanning electron microscope and insert of the micrograph showing corrosion products deposited under the pillar-implant connection.

Table 2
Semi-quantitative composition in % mass of the corrosion product deposit on the pillar-implant connection measured using energy dispersive spectroscopy technique in an electron scanning microscope.

Elements	Mass (%)
Ti	22.87
Fe	15.85
Na	13.86
Cl	13.24
C	12.13
O	8.12
Cr	4.86
P	4.12
Ni	3.14
V	1.06
Mo	0.74

used in the galvanic coupling since the junction of Ti with Au is more resistant to galvanic and crevice corrosion than the coupling of Ti with non-precious metals that presented high susceptibility to crevice corrosion.

Taher et al. [46] evaluated the galvanic corrosion behavior of Co-Cr, Ni-Cr, Ag-Pd, Au and Ti ternary alloys coupled to a Ti abutment in artificial saliva. The results showed that the gold alloy did not present susceptibility to galvanic coupling with Ti implant. The Co-Cr alloy R2000 was the least acceptable combination in terms of resistance to galvanic corrosion and the amalgam showed galvanic interaction, not being recommended to use these two materials in the oral region.

Quezada-Castillo et al. [47] performed a study of galvanic corrosion between Ti-6Al-4V alloy and with Co-Cr or Ni-Cr in aerated artificial saliva using electrochemical techniques such as open circuit potential and potentiodynamic polarization curves. The results of galvanic coupling between the Ti alloy and Co-Cr were more resistant to corrosion than the coupling between Ti-6Al-4V and Ni-Cr.

According to Oh et al. [4], one of the corrosion mechanisms that can occur at the pillar-implant interface is crevice corrosion, since the joining of the two materials (implant and prosthetic abutment) can result in a region with low oxygen availability and thus, an increased concentration of metal ions in solution, favoring a decrease in local pH. Thus, with the immersion time, the TiO_2 film becomes weakened, leading to corrosion acceleration, corroborating the results of this study.

5. Conclusions

The electrochemical behavior of samples of Ti-6Al-4V dental implant connected to stainless steel AISI 316 L prosthetic abutment was investigated in solution that simulate inflammatory and crevice conditions. The assembly of the two alloys was carried out using mechanical imbrication by means of successive strikes at 0.05 J force onto the abutment inserted in the implant along the centerline two alloys using either 3 strikes, 5 strikes or 7 strikes. The results led to the following conclusions:

1. The Ti-6Al-4V alloy acted as anode whereas the stainless steel as cathode in the galvanic couple.
2. The susceptibility to localized attack at the interface between the two alloys increased as the number of strikes decreased and this was related to the gap, either width or depth, between the two alloys.
3. The increased resistance to localized attack at the boundary between the two alloys with the increased number of strikes was supported by all the electrochemical tests carried out and by analysis of the exposed surface after tests by electrochemical microscopy and visual observation.
4. The use of local electrochemical techniques proved very useful in evaluating the corrosion of dental implants made with different metallic materials leading to galvanic coupling.

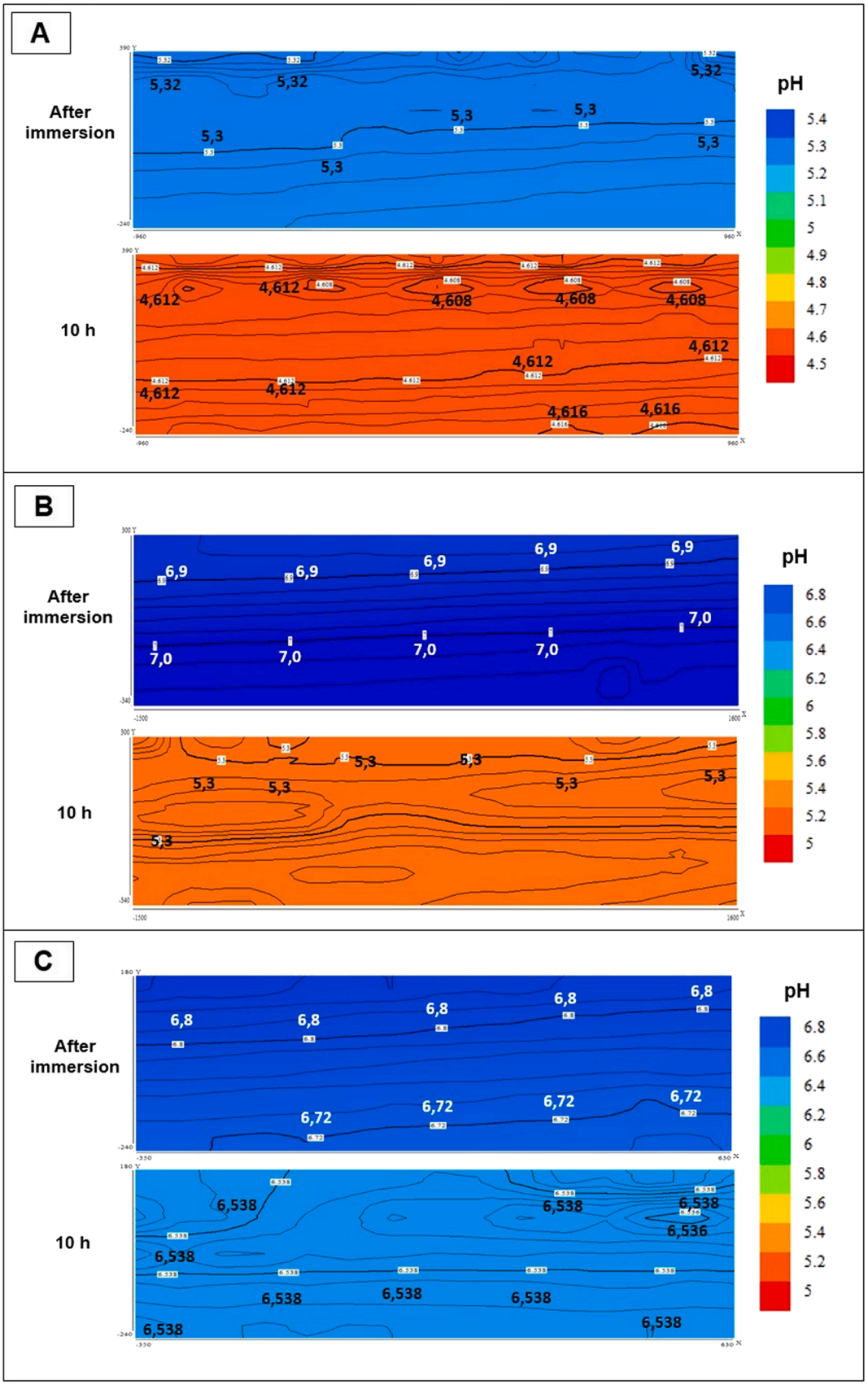

Fig. 9. Local pH maps of the longitudinal section of the abutment-implant interface for samples connected with 3 (A), 5 (B) and 7 strikes (C) after immersion (15 min) and after 10 h in PBS solution with 1% (v) of H_2O_2 and pH-adjusted in 7.0. Area (1 ×2.5) mm^2.

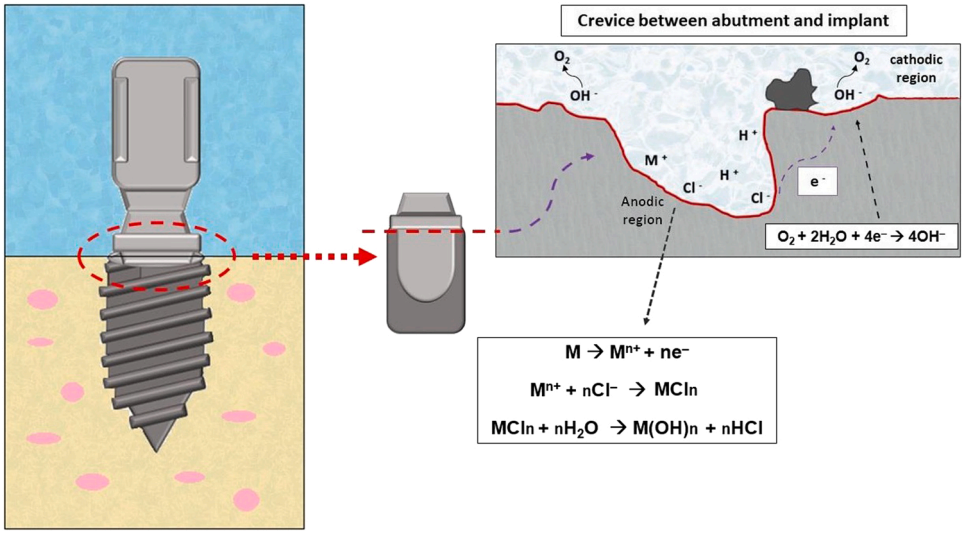

Fig. 10. Illustration of the samples with the abutment (AISI 316 L) and the implant (Ti-6Al-4V) connected and the gap between the two materials leading to a mechanism of crevice corrosion.

Funding

This work was supported by CAPES [PROEX nº 88882.333456/2019-01]; and the IPEN/CNEN for financial support [Edital Intercentros IPEN 05/2018–2018.05. IPEN.06].

CRediT authorship contribution statement

Larissa Oliveira Berbel: Conceptualization, Methodology, Validation, Investigation, Resources, Writing – original draft, Visualization, Funding acquisition. **Bárbara Victoria Gonçalves de Viveiros:** Methodology, Validation, Investigation. **Ana Lígia Piza Micelli:** Conceptualization, Writing – review & editing. **Frederico Nigro:** Conceptualization, Writing – review & editing. **Jesualdo Luiz Rossi:** Conceptualization, Writing – review & editing, Supervision. **Isolda Costa:** Methodology, Conceptualization, Writing – review & editing, Supervision, Funding acquisition.

Declaration of Competing Interest

The authors declare that they have no known competing financial interests or personal relationships that could have appeared to influence the work reported in this paper.

Data Availability

Data will be made available on request.

Acknowledgments

The authors would like to thank CAPES for the scholarship to L.O Berbel. They are also grateful for the support of the Multiuser Laboratory of the Center for Lasers and Applications at IPEN-CNEN/SP and the Microscopy and Microstructure Laboratory (LMM/IPEN). The authors are indebted to FGM System - Brazil, for implants supply.

References

[1] A. Ravoiu, L. Benea, A. Chiriac. Metabolic albumin and its effect on electrochemical behavior on titanium implant alloy. IOP Conference Series: *Materials Science and Engineering*, Euroinvent ICIR 2018, 17–18 May, 2018, Iasi, Romania, 374 (2018) pp. 1–8.

[2] X. Chen, K. Shah, S. Dong, L. Peterson, E.C. La Plante, G. Sant. Elucidating the corrosion-related degradation mechanisms of Ti-6Al-4V dental implants, Dent. Mater. 36 (2020) 431–441, https://doi.org/10.1016/j.dental.2020.01.008.

[3] A.L.P. Micelli, F. Nigro, C.S. Mucsi, M. Cavalieri, L.C. Aranha, J.L.Rossi Analysis, of the pullout testing of straight and angled abutments in narrow diameter implants, Mater. Sci. Forum 1012 (2020) 461–465, https://doi.org/10.4028/www.scientific.net/MSF.1012.461.

[4] K.-T. Oh, K.-N. Kim, Electrochemical properties of suprastructures galvanically coupled to a titanium implant, J. Biomed. Mater. Res. Part B Appl. Biomater. 2 (2004) 318–331, https://doi.org/10.1002/jbm.b.30046.

[5] G.E. Romanos, G.A. Fischer, R. Delgado-Ruiz. Titanium wear of dental implants from placement, under loading and maintenance protocols, Int. J. Mol. Sci. 22 (2021) 1–19, https://doi.org/10.3390/ijms22031067.

[6] M. Alshehri, H.A. Antimicrobial, efficacy of materials used for sealing the implant abutment screw hole: an in vitro evaluation, Implant Dent. 26 (2017) 911–914, https://doi.org/10.1097/ID.0000000000000688.

[7] P.P. Binon, Implants and components: entering the new millennium, Int. J. Oral. Maxillofac. Implants 15 (1) (2000) 76–94.

[8] C. Sahin, S. Ayyildiz, Correlation between microleakage and screw loosening at implant-abutment connection, J. Adv. Prosthodont. 6 (1) (2014) 35–38, https://doi.org/10.4047/jap.2014.6.1.35.

[9] C. Nascimento, P.K. Miani, V. Pedrazzi, R.B. Gonçalves, R.F. Ribeiro, A.C.L. Faria, A.P. Macedo, R.F. Albuquerque Jr., Leakage of saliva through the implant-abutment interface: In Vitro evaluation of three different implant connections under unloaded and loaded conditions, Int. J. Oral. Maxillofac. Implants 27 (3) (2012) 551–560.

[10] D. Weng, M.J.H. Nagata, M. Bell, A.F. Bosco, L.G.N. Melo, E.-J. Richter, Influence of microgap location and configuration on the periimplant bone morphology in submerged implants. An experimental study in dogs, Clin. Oral. Implants Res. 19 (11) (2008) 1141–1147, https://doi.org/10.1111/j.1600-0501.2008.01564.x.

[11] R.M. Shadid, N.R. Sadaqah, L. Abu-naba'a, W.M.Al-Omari Comparison, between the butt-joint and Morse taper implant-abutment connection: a literature review, J. Implant Adv. Clin. Dent. 5 (10) (2013) 33–40.

[12] J.M. Cordeiro, T. Beline, A.L.R. Ribeiro, E.C. Rangel, N.C. Cruz, R. Landers, L. P. Faverani, L.G. Vaz, L.M.G. Fais, F.B. Vicente, C.R. Grandini, M.T. Mathew, C. Sukotjo, V.A.R. Barão, Development of binary and ternary titanium alloys for dental implants, Dent. Mater. 33 (2017) 1244–1257, https://doi.org/10.1016/j.dental.2017.07.013.

[13] A.R. Coppedè, E. Bersani, M.G.C. Mattos, R.C.S. Rodrigues, I.A.M. Sartori, R. F. Ribeiro, Fracture resistance of the implant-abutment connection in implants with internal hex and internal conical connections under oblique compressive loading: an in vitro study, Int J. Prosthodont 22 (3) (2009) 283–286.

[14] D. Bozkaya, S. Müftü, Mechanics of the taper integrated screwed-in (TIS) abutments used in dental implants, J. Biomech. 38 (1) (2005) 87–97, https://doi.org/10.1016/j.jbiomech.2004.03.006.

[15] I.C. Moris, A.C. Faria, M.G. Mattos, R.F. Ribeiro, R.C. Rodrigues, Mechanical analysis of conventional and small diameter conical implant abutments, J. Adv. Prosthodont. 4 (3) (2012) 158–161, https://doi.org/10.4047/jap.2012.4.3.158.

[16] W.M. Peruzetto, E.F. Martinez, D.C. Peruzzo, J.C. Joly, M.H. Napimoga, Microbiological seal of two types of tapered implant connections, Braz. Dent. J. 27 (3) (2016) 273–277, https://doi.org/10.1590/0103-6440201600604.

[17] J.P. Aloise, R. Curcio, M.Z. Laporta, L. Rossi, A.M.A. Silva, A. Rapoport, A. Microbial leakage through the implant-abutment interface of morse taper implants in vitro, Clin. Oral. Implants Res. 21 (3) (2010) 328–335, https://doi.org/10.1111/j.1600-0501.2009.01837.x.

[18] H. Hung, C.-S. Huang, Y.-H. Pan, The compressive strength of implant-abutment complex with different connection designs, J. Dent. Sci. 14 (3) (2019) 318–324, https://doi.org/10.1016/j.jds.2019.01.014.
[19] S. Harder, E.S. Quabius, L. Ossenkop, M. Kern, Assessment of lipopolysaccharide microleakage at conical implant-abutment connections, Clin. Oral. Investig. 16 (5) (2012) 1377–1384, https://doi.org/10.1007/s00784-011-0646-4.
[20] F. Bajoghli, M. Amjadi, M. Akouchekian, T. Narimani, Bacterial leakage and microgap along implant-abutment connection in three different implant systems, Int. J. Adv. Biotechnol. Res. IJBR 7 (4) (2016) 1284–1290.
[21] R. Faria, L.G. May, D.K. Vasconcellos, C.A.M. Volpato, M.A. Bottino, Evaluation of the bacterial leakage along the implant-abutment interface, J. Dent. Implants 1 (2) (2011) 51–57, https://doi.org/10.4103/0974-6781.91280.
[22] L. Baggi, M. Girolamo, C. Mirisola, R. Calcaterra R, Microbiological evaluation of bacterial and Mycotic seal in implant systems with different implant-abutment interfaces and closing torques values, Implant Dent. 22 (4) (2013) 344–350, https://doi.org/10.1097/ID.0b013e3182943062.
[23] D.C.C. Alves, P.S.P. Carvalho, C.N. Elias, E. Vedovatto, E.F. Martinez, In vitro analysis of the microbiological sealing of tapered implants after mechanical cycling, Clin. Oral. Investig. 20 (9) (2016) 2437–2445, https://doi.org/10.1007/s00784-016-1744-0.
[24] J.S. Guindy, H. Schiel, F. Schmidli, J. Wirz, Corrosion at the marginal gap of implant-supported suprastructures and implant failure, Int. J. Oral. Maxillofac. Implants 19 (6) (2004) 826–831.
[25] T.Q. Ansari, J.-L. Luo, S.-Q. Shi, Modeling the effect of insoluble corrosion products on pitting corrosion kinetics of metals, Mater. Degrad. 3 (28) (2019) 1–12, https://doi.org/10.1038/s41529-019-0090-5.
[26] J. Izquierdo, G. Bolat, D. Mareci, C. Munteanu, S. González, R.M. Souto, Electrochemical behaviour of Zr-Ti alloys in artificial physiological solution simulating in vitro inflammatory conditions, Appl. Surf. Sci. 313 (2014) 259–266, https://doi.org/10.1016/j.apsusc.2014.05.201.
[27] R. Bhola, S.M. Bhola, B. Mishra, D. Olson, Corrosion in titanium dental implants/prostheses - a review, Trends Biomater. Artif. Organs 25 (1) (2011) 34–46.
[28] L.O. Berbel, E.P. Banczek, I.K. Karoussis, G.A. Kotsakis, I. Costa, Determinants of corrosion resistance of Ti-6Al-4V alloy dental implants in an in vitro model of peri-implant inflammation, PLoS ONE 14 (1) (2019) 1–17, https://doi.org/10.1371/journal.pone.0217671.
[29] A. Sadaqat, A.M.A. Rani, K. Altaf, P. Hussain, C. Prakash, S. Hastuty, T.V.V.L. N. Rao, A.A. Aliyu, K. Subramaniam. Investigation of alloy composition and sintering parameters on the corrosion resistance and microhardness of 316L stainless steel alloy, in: B. Gapiński, M. Szostak, V. Ivanov (Eds.), Advances in Manufacturing II. MANUFACTURING 2019. Lecture Notes in Mechanical Engineering, Springer, Cham, 2019, pp. 532–541, https://doi.org/10.1007/978-3-030-16943-5_45.
[30] U. Eduok, J. Szpunar, In vitro corrosion studies of stainless-steel dental substrates during Porphyromonas Gingivalis biofilm growth in artificial saliva solutions: providing insights into the role of resident oral bacterium, RSC Adv. 10 (2020) 31280–31294, https://doi.org/10.1039/d0ra05500j.
[31] Arcsys Implant System. Available at ⟨https://fgmdentalgroup.com/arcsys/⟩ (accessed 15th July 2021). (In Portuguese).
[32] ASTM F1108 - 14 Standard Specification for Ti6Al4V Alloy Castings for Surgical Implants (UNS R56406).
[33] M. Guo, L. Liu, J. Zhang, M. Liu, Role of reactive oxygen species and advanced glycation and products in the malfunctioning of dental implants, West Indian Med. J. 64 (4) (2015) 419–423, https://doi.org/10.7727/wimj.2014.105.
[34] S. Nasrazadani, S. Hassani, Modern analytical techniques in failure analysis of aerospace, chemical, and oil and gas industries.. Handbook of Materials Failure Analysis with Case Studies from the Oil and Gas Industry, Butterworth-Heinemann,, 2016, pp. 39–54, https://doi.org/10.1016/B978-0-08-100117-2.00010-8.
[35] G. Bolat, J. Izquierdo, J.J. Santana, D. Mareci, R.M. Souto, Electrochemical characterization of ZrTi alloys for biomedical applications, Electrochem. Acta 88 (2013) 447–456, https://doi.org/10.1016/j.electacta.2012.10.026.
[36] V. Gentil. *Corrosão*. LTC - Livros Técnicos e Científicos Editora S.A. 3th Edition (1998). (In Portuguese).
[37] H. Kaminaka, S. Matsumoto, H. Kamio, Characteristics and applications of high corrosion resistant titanium alloys, Nippon Steel Sumitomo Met. Tech. Rep. 106 (2014) 24–40.
[38] D. Prando, A. Brenna, M.V. Diamanti, S. Beretta, F. Bolzoni, M. Ormellese, M. Pederetti. Corrosion of titanium: Part 1: aggressive environments and main forms of degradation, J. Appl. Biomater. Funct. Mater. 15 (4) (2017) 291–302, https://doi.org/10.5301/jabfm.5000387.
[39] E.M. Anwar, L.S. Kheiralla, R.H. Tamman, Effect of fluoride on the corrosion behavior of Ti and Ti6Al4V dental implants coupled with different superstructure, J. Oral. Implantol. 37 (1) (2011) 309–317, https://doi.org/10.1563/AAID-JOI-D-09-00084.
[40] L. Geis-Gerstorfen, J.G. Weber, K.H. Sauer, In vitro substance loss due to galvanic corrosion in titanium implant/Ni-Cr supraconstruction system, Int. J. Oral. Maxillofac. Implants 9 (1994) 449–454.
[41] N. Rashidi, S. Alavi-Soltani, R. Asmatulu. Crevice corrosion theory, mechanisms and prevention methods. In: *3rd Annual Symposium: Graduate Research and Scholarly Projects*, Whichita, KS: Wichita State University (2007) pp. 215–216.
[42] W.F. Smith, J. Hashemi. Foundations of Materials Science and Engineering, fourth ed., McGraw - Hill Book,, 2006.
[43] A. Al'Otaibi, E.M. Sherif, S. Zinelis, Y.S.Al'Jabbari Corrosion, behavior of two cp titanium dental implants connected by cobalt chromium metal superstructure in artificial saliva and the influence of immersion time, Int. J. Electrochem. Sci. 11 (2016) 5877–5890, https://doi.org/10.20964/2016.07.77.
[44] L. Reclaru, J.M. Meyer, Study of corrosion between a titanium implant and dental alloys, J. Dent. 22 (3) (1994) 159–168, https://doi.org/10.1016/0300-5712(94)90200-3.
[45] A. Mellado-Valero, A.I. Muñoz, V.G. Pina, M.F. Sola-Ruiz, Electrochemical behaviour and galvanic effects of titanium implants couples to metallic suprastructures in artificial saliva, Materials 11 (1) (2018) 1–19, https://doi.org/10.3390/ma11010171.
[46] N.M. Taher, A.S. Al Jabab, Galvanic corrosion behavior of implant suprastructure dental alloys, Dent. Mater. 19 (2003) 54–59, https://doi.org/10.1016/S0109-5641(02)00008-8.
[47] E. Quezada-Castillo, W. Aguilar-Castro, B. Quezada-Alván, Corrosion of galvanic couplings of Ni-Cr and Co-Cr alloys with Ti-6Al-4V in artificial saliva using electrochemical methods, Rev. Matér. 25 (1) (2020) 6–11, https://doi.org/10.1590/S1517-707620200001.0926.